# Design Sensor Trajectory for Control: Application to Sheet-Forming Processes

**Der-Ming Chang, Cheng-Ching Yu, and I-Lung Chien**
Dept. of Chemical Engineering, National Taiwan University of Science and Technology, Taipei 106-07, Taiwan

*The conventional scanning sensor generates a zig-zag pattern for the sheet-forming process, immediately leading to the problem of unequal measurement update intervals in state estimation. Instead of reconstructing the profile given a zig-zag pattern, the sensor trajectory was redesigned to better estimation and control. In this work, the characteristics of the conventional scanning sensor were explored as well as the implications in estimation and control. The concept of elliptic sensor contour is presented, deriving analytical expressions for the sensor trajectories. Alternatively, the improved sensor trajectory can be obtained using a variable-speed scanning sensor under linear sweep. That implies that control performance can be improved by reprogramming the motor of the existing sensor. Moreover, several alternatives for sensor arrangement are also explored. The results for estimation and control can be used as guidelines for the development of future sensor technology.*

## Introduction

Sheet forming is an important unit operation in many manufacturing processes. Common examples include papermaking, metal rolling, polymer film extrusion, and coating. The control objective of these processes is to maintain the quality uniformity of the end products, for example, rolls of paper sheets or polymer films. Therefore, we are controlling two-dimensional (2-D) products and the major concern is the quality variations occurring in the direction of flow, the machine direction (MD), and perpendicular to the direction of flow, the cross direction (CD). The last decade has seen advances in CD control. Linear quadratic Gaussian (LQG) types of controllers are employed to achieve uniformity in the cross direction (Chen and Wilhelm, 1986; Bergh and MacGregor, 1987). Various model predictive control (MPC) strategies for such a large-scale system were also proposed (Braatz et al., 1992; Laughlin et al., 1993; Rawlings and Chien, 1996; Dave et al., 1997; Dave et al., 1999; Van Antwerp and Braatz, 2000). In order to maintain the uniformity of some properties, for example, basis weight and thickness, across the sheet, the control strategies rely on the measurement of the property along both the CD and MD directions. The sensor of interest is the gauge sensor. It normally consists of a radiation-emitting source and a detector. The property (such as thickness) of the film is sensed by the attenuation of the radiation signal.

The sensor is often arranged as a scanning device mounted on a carriage that moves back and forth in the cross direction. Since the film is moving in the machine direction, this generates a zig-zag pattern on the film (Figure 1). This immediately leads to the following question: How does one reconstruct the full two-directional profile, given only a zig-zag pattern on the film. The Kalman filter is the natural choice for the state estimation problem as discussed by several authors (Bergh and MacGregor, 1987; Chen, 1992; Wang et al., 1993; Tyler and Morari, 1995; Rawlings and Chien, 1996). Rigopoulos et al. (1997) use the Karhunen-Loève expansion to identify the significant features, followed by the autoregressive model to reconstruct the temporal model. Recently, we have also seen rapid development in alternative sensor technologies. This includes the full array wet or dry end sensor (Shapiro, 1998), additional dry end sensors (Tyler and Morari, 1995), and the full-sheet imaging system (Chen and Pfeifer, 1998).

This work differs and complements the previous work in that the main objective is to investigate the effect of the zig-zag pattern on control performance. Moreover, we go a step further by changing the pattern of the process measurements such that better control performance can be achieved. The

Correspondence concerning this article should be addressed to C.-C. Yu.

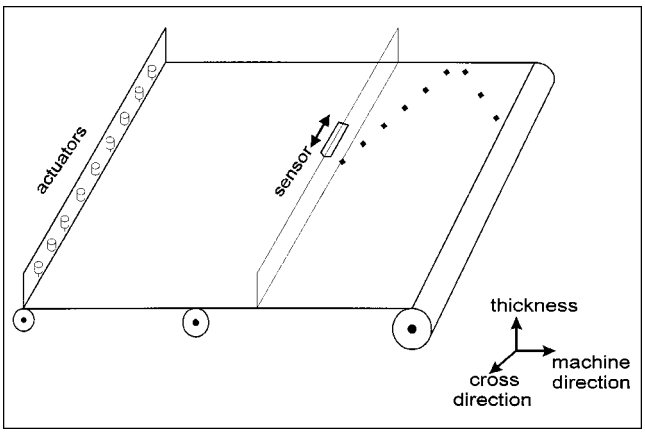


**Figure 1. Sheet forming process.**

remainder of this article is organized as follows. The modeling and estimation problems are addressed in the second section. The third section discusses the optimal estimation in the temporal mode, plus it explores the effects on control performance. In the fourth section approaches to improve the measurement pattern for better control are given and alternative sensor arrangements also are explored, followed by the conclusion.

## Process Modeling and Characteristics

Before getting into the process modeling, let us look at the measurement pattern as the scanning sensor moves along the cross directions (such as Figure 1). Assume the sensor moves with a fixed speed ($v_s$) and the speed in the machine direction ($v_p$) is also constant. Then we have a linear measurement profile as the sensor sweeps forward (such as the measured points between $60 \le \text{time} \le 70$ in Figure 2A) and, on the return path, we obtain another linear trajectory, as shown in Figure 2A ($70 \le \text{time} \le 80$). This is exactly the zig-zag trajectory mentioned in the literature. Since the scanning sensor moves back and forth with the same speed, the zig-zag profile repeats itself over the entire sheet. Rawlings and Chien (1996) point out that the correctness of the estimation is affected by this particular pattern. The effects of the profile on estimation and control can be analyzed by examining a single period (such as $T$ in Figure 2A) of the periodical function. Several observations can be made immediately.

Consider a period $T$ in which two measurement updates are made.

1. On a given position in the CD, two immediate measurement updates result in a constant time period $T$. This is $T = T_1 + T_2$, where $T_1$ and $T_2$ are the times to the first and second measurement updates (Figure 2).

2. For two subsequent measurements, the elapsed times until the next measurement update are not the same ($T_1 \neq T_2$) except for the center (Figure 2).

3. The difference between the time interval (that is, $|T_1 - T_2|$) is small around the center and becomes larger toward the edges (Figure 2B).

Therefore, we have a periodical function. In each period $T$ two measurement updates are made over the intervals $T_1$ and $T_2$, respectively, and generally $T_1 \neq T_2$.

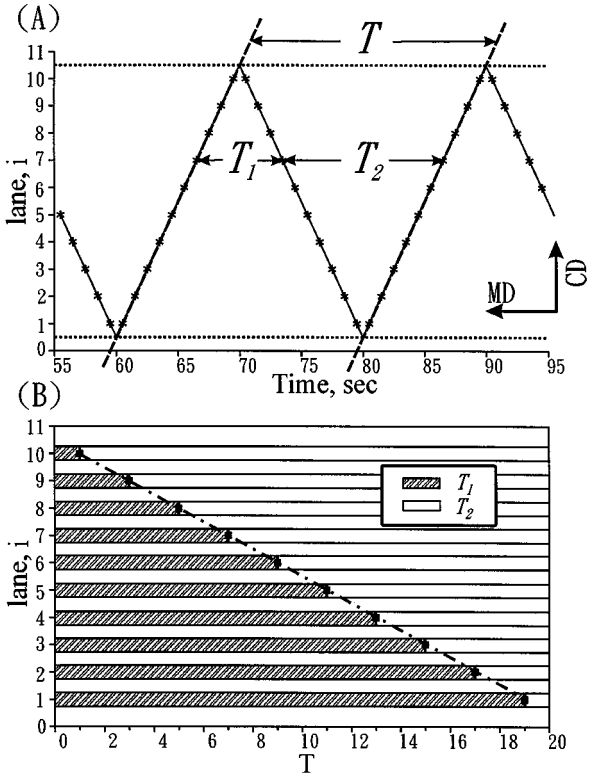


**Figure 2. Scanning sensor in linear sweep.**

(A) zig-zag sensor trajectory and (B) distribution of measurement update intervals ($T_1$ and $T_2$).

### *Modeling*

The goal of modeling is to provide the simplest mathematical model that can describe the essential features of the sampling mechanism. Following the approach of Bergh and MacGregor (1987), a linear time-invariant (LTI) dynamic model is employed.

$$\dot{x}(t) = A_c x(t) + B_c u(t) + w_c(t), \qquad t \in [0, \infty), \qquad (1)$$

where $x$ is a vector of the state variables, $u$ is the process input, the subscript $c$ denotes the continuous time system, and $w_c$ is white noise with zero mean and the strength is described by a covariance matrix:

$$E\{w_c(t) w_c(\tau)^T\} = Q_c \delta(t - \tau), \qquad (2)$$

where $E\{\cdot\}$ denote the expectation, $\delta(t)$ is Kronecker delta, and $Q_c$ is a positive semidefinitive covariance matrix. Equations 1 and 2 describe the continuous time system. The discrete time model is useful in applications. If we allow the sampling time to vary, it becomes a time-varying system

$$x[k+1] = A[k]x[k] + B[k]u[k] + w[k] \qquad (3)$$

$$y[k] = C[k]x[k] + v[k], \qquad (4)$$

where $v(k)$ is the measurement noise with a covariance $R$. The relationship between continuous-time and discrete-time model parameters (such as $A$, $B$, $C$) can be found elsewhere

(Mayback, 1979). Many authors use Eqs. 3 and 4 to represent the process where $A$ and $B$ matrices are often assumed to be constant and a time-varying $C(k)$ is employed. The $C(k)$ is a vector with an entry 1 corresponding to the current measured state and 0 elsewhere (Bergh and MacGregor, 1987; Tyler and Morari, 1995; Rawlings and Chien, 1996).

## Kalman filtering

The Kalman filter is effective in state reconstruction. The Kalman filter algorithm has the following steps (Bryson and Ho, 1975; Grewal and Andrews, 1993):

1. Compute the *a priori* state estimation $\hat{x}[k|k-1]$:

$$\hat{x}[k|k-1] = A[k]\hat{x}[k-1|k-1] + B[k]u[k-1]. \quad (5)$$

2. Extrapolate the error covariance $\Sigma_e$ ($\Sigma_e[k|k-1] = e[k|k-1]e^T[k|k-1]$, where $e[k|k-1] \equiv x[k] - \hat{x}[k|k-1]$):

$$\Sigma_e[k|k-1] = A[k]\Sigma_e[k-1|k-1]A[k]^T + Q[k]. \quad (6)$$

3. Compute the filter gain matrix ($K[k]$):

$$K[k] = \Sigma_e[k|k-1]C[k]^T\left(C[k]\Sigma_e[k|k-1]C^T[k] + R[k]\right)^{-1}. \quad (7)$$

4. Update the *posteriori* state estimation $\hat{x}[k|k]$ once the measurement becomes available:

$$\hat{x}[k|k] = \hat{x}[k|k-1] + K[k]\left(y[k] - C[k]\hat{x}[k|k-1]\right). \quad (8)$$

5. Update the error covariance:

$$\Sigma_e[k|k] = (I - K[k]C[k])\Sigma_e[k|k-1] \quad (9)$$

Let us use a simple example to illustrate the effect of sampling time ($T_s$) on the error covariance ($\Sigma_e$). Consider a simple LTI system

$$\dot{x}(t) = -0.05x(t) + w_c(t) \quad (10)$$

$$y(t_k) = x(t_k) + v(t_k), \quad (11)$$

where the strength of the process and measurement noises are 1 and 0.01, respectively. Figure 3A shows that right after a measurement update, the error covariance increases (c.f. Eq. 6) until the next measurement becomes available. Therefore, for the system with the fixed $T_s$, the worst estimation error (in terms of variance) is proportional to the sampling time, as shown in Figure 3A.

The Kalman filter can also be utilized to analyze our sampling problem: a fixed period ($T$) with two measurement update intervals $T_1$ and $T_2$. Again, consider the simple system in Eqs. 10 and 11 with $T = 6$. If $T_1$ and $T_2$ are equally spaced (that is, $T_1 = T_2$), the worst error variances in estimation are approximately the same at each interval. However, if $T_1 \neq T_2$ (such as, $T_1 = 4$ and $T_2 = 2$), then the worst error variance is larger than that of the $T_1 = T_2$ case (Figure 3B). Figure 3B also reveals that the error covariances increase until the next

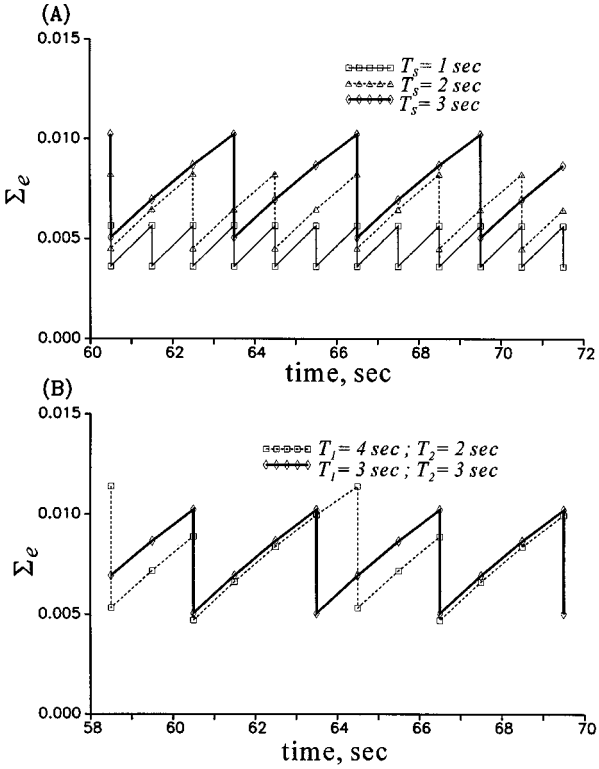


**Figure 3. Variances of Kalman filter estimation.**

(A) Different sampling times and (B) different measurement update intervals ($T_1$ and $T_2$) for a constant full period ($T = T_1 + T_2$).

measurement update and magnitude of the error is proportional to the sampling interval (such as $T_1$ or $T_2$). As the system becomes stationary, the characteristics in Figure 3B repeat exactly the same pattern (Mayback, 1979).

First, let us focus on the error covariance of a specific CD position. This is similar to a single state system with two different sampling times. The error covariance right before the measurement update can be derived. Consider a system with a period of $T$ and two sampling intervals $T_1$ and $T_2$ (that is, the first measurement comes in at time $T_1$ and the second measurement is available at $T_2$ after that). That gives a system with time-varying $A$ and $B$ and a constant $C$ (Eqs. 3 and 4). From Eqs. 6 and 9, the error covariances before and after the measurement update are

$$\Sigma_{e,1}[k|k-1] = A_1^2\Sigma_{e,2}[k-1|k-1] + Q_1 \quad (12)$$

$$\Sigma_{e,1}[k|k] = (1 - K_1)\Sigma_{e,1}[k|k-1] \quad (13)$$

and

$$\Sigma_{e,2}[k|k-1] = A_2^2\Sigma_{e,1}[k-1|k-1] + Q_2 \quad (14)$$

$$\Sigma_{e,2}[k|k] = (1 - K_2)\Sigma_{e,2}[k|k-1], \quad (15)$$

where the subscripts 1 and 2 denote the first or second measurement update. Since we are using the same scanning sen-

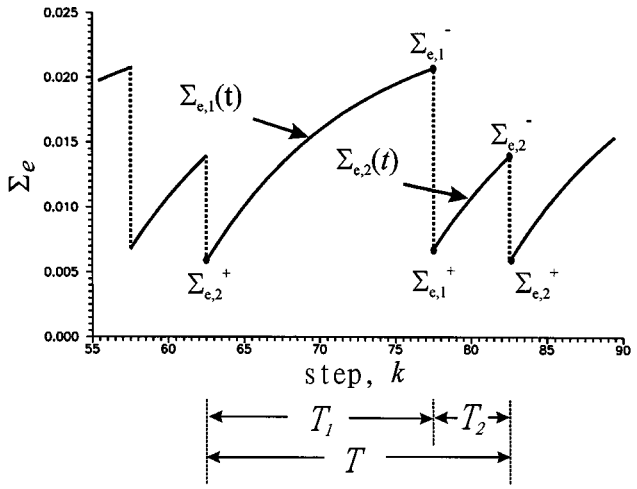


**Figure 4. Variance of estimation before the after measurement updates.**

sor with a noise covariance $R$, the filter gain ($K_i$) becomes

$$K_i = \frac{\Sigma_{e,i}[k|k-1]}{\Sigma_{e,i}[k|k-1] + R}. \tag{16}$$

The error covariances can be expressed analytically in terms of system parameters. Let $\Sigma_{e,i}^-$ and $\Sigma_{e,i}^+$ denote the covariances right before and after the measurement udpate, as shown in Figure 4. A quadratic function in $\Sigma_{e,i}^+$ (or $\Sigma_{e,i}^-$) can be obtained by rearranging Eqs. 12–16. After some algebraic manipulation, $\Sigma_{e,i}^+$ can be expressed as

$$\Sigma_{e,i}^+ = \frac{-b_i^+ + \sqrt{(b_i^+)^2 - 4a_i^+ c_i^+}}{2a_i^+}, \tag{17}$$

where

$$a_i^+ = A_j^2\left(A_i^2 R + Q_i + R\right), \qquad j \neq i \tag{18}$$

$$b_i^+ = A_i^2 Q_j R + (Q_i + R)(Q_j + R) - A_i^2 A_j^2 R^2 - A_j^2 Q_i R \tag{19}$$

$$c_i^+ = -\left[A_i^2 Q_j R^2 + (Q_j + R) Q_i R\right], \tag{20}$$

where $A_i$ and $Q_i$ denote $A(T_i)$ and $Q(T_i)$ of Eq. 3. Similarly, the extrapolated error covariance right before the update ($\Sigma_{e,i}^-$) can also be derived:

$$\Sigma_{e,i}^- = \frac{-b_i^- + \sqrt{(b_i^-)^2 - 4a_i^- c_i^-}}{2a_i^-}, \tag{21}$$

with

$$a_i^- = A_j^2 R + Q_j + R \tag{22}$$

$$b_i^- = (Q_j + R)(R - Q_j) - A_i^2 A_j^2 R^2 - A_i^2 Q_j R - A_j^2 Q_i R \tag{23}$$

$$c_i^- = -\left[A_i^2 Q_j R^2 + (Q_j + R) Q_i R\right]. \tag{24}$$

Certainty, for a given system, the expression of the error covariance as a function of time can also be obtained:

$$\Sigma_{e,i}(t) = \Phi^2(t,0)\Sigma_{e,j}^+ + \int_0^t \Phi^2(t,\tau) Q_c \, d\tau, \qquad 0 \le t \le T_i, \tag{25}$$

where $\Phi$ is the state transition matrix (Mayback, 1979) when a sampling time of $T_i$ is used. The results indicate that $\Sigma_e(t)$ is a piecewise continuous function (Figure 4). The results (Eqs. 17, 21, and 25) shown here are useful in evaluating the effect of different sampling intervals on the estimation and control.

## Estimation and Control

### *Estimation: optimal sampling interval*

The ongoing analyses show that for a given full period and two measurement updates, the error covariance [that is, $\Sigma_{e,i}(t)$] is a function of the sampling intervals ($T_i's$). In this section, we explore the effect of the unequal sampling interval on the estimation. Consider a scanning system with a full period $T$ and two measurement updates at time intervals $T_1$ and $T_2$:

$$T = T_1 + T_2. \tag{26}$$

The objective function we are interested in is the integrated square error of the estimation

$$J = \int_0^{T_1} \Sigma_{e,1}(t)\, dt + \int_0^{T_2} \Sigma_{e,2}(t)\, dt. \tag{27}$$

We would like to find the measurement update interval ($T_1$) such that the estimation error is minimized:

$$\min_{0 < T_1 < T} J. \tag{28}$$

The result can be obtained by taking the derivative of $J$ with respect to $T_1$. The result shows that, in terms of square error, the least estimation error corresponds to the following sampling interval:

$$T_1 = \frac{T}{2}. \tag{29}$$

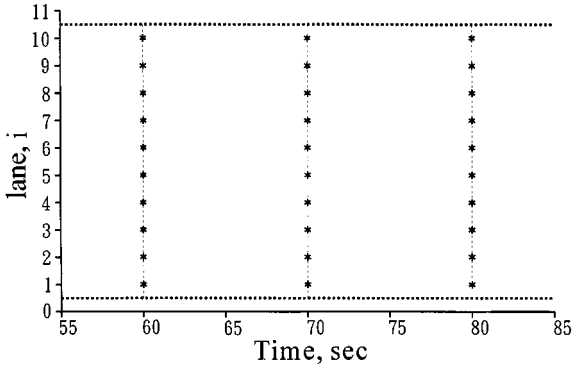


**Figure 5. Sensor trajectory for stationary sensors with a large sampling interval ($T/2$).**

The derivation is given in the Appendix. The result indicates that the minimum estimation error occurs when the sampling intervals (that is, $T_1$ and $T_2$) are equally spaced. This confirms our physical intuition. Similarly, for the case of the worst ($\infty$-norm) estimation error, the statement of the problem becomes

$$\min_{0<T_1<T} \max\left(\Sigma_{e,1}^{-}, \Sigma_{e,2}^{-}\right). \tag{30}$$

Since $\Sigma_{e,1}^{-}$ and $\Sigma_{e,2}^{-}$ are symmetrical with respect to the measurement update interval and $\Sigma_{e,i}(t)$ is a monotonically increasing function, the minimum exists when $T_1 = T/2$. In other words, for each lane in the cross direction, better estimation can be achieved when the two measurement update intervals are closed to each other. Obviously, the zig-zag pattern (Figure 2) of the scanning sensor is far different from the ideal situation.

### *Estimation: Deviation from the optimal estimation*

The measurement pattern giving the optimal estimation, with equally spaced measurement update intervals, can be viewed as the case of stationary sensors with a sampling period of $T/2$. Figure 5 shows the measurement pattern. Here, we are interested in the performance degradation (increase in the estimation error) of the scanning sensor as compared to the ideal system, the stationary system with the same number of measurements. Notice that this is strictly a temporal consideration.

Consider a system with 10 lanes in the CD. The dynamic system is modeled as Eqs. 1 and 2 with $A_c = -0.05I$ (where $I$ is an identity matrix) and $B_c = 0.05I$. The process noise is described by the covariance matrix:

$$Q = \begin{bmatrix} 1 & \rho_s & \rho_s^2 & \cdots & \rho_s^{n-1} \\ & 1 & \rho_s & \cdots & \rho_s^{n-2} \\ & & \ddots & & \vdots \\ & & & \ddots & \rho_s \\ \text{sym.} & & & & 1 \end{bmatrix} \sigma_{w,c}^2. \tag{31}$$

For the moment let us assume $\rho_s = 0$ and $\sigma_{w,c}^2 = 1$. The sampling time is 1 with a noise level of 0.01 (Eq. 4). For the scanning sensor the measurement matrix $C[k]$ is time-varying. In a full period $T$ with $2n$ measurements, the stacked $C$ matrices becomes

$$\begin{bmatrix} C[1] \\ C[2] \\ \vdots \\ C[n] \\ \hline C[n+1] \\ C[n+2] \\ \vdots \\ C[2n] \end{bmatrix} = \left[\begin{array}{ccccccc} 1 & 0 & 0 & \cdots & 0 & 0 & 0 \\ 0 & 1 & 0 & \cdots & 0 & 0 & 0 \\ & & & \vdots & & & \\ 0 & 0 & 0 & \cdots & 0 & 0 & 1 \\ \hline 0 & 0 & 0 & \cdots & 0 & 0 & 1 \\ 0 & 0 & 0 & \cdots & 0 & 1 & 0 \\ & & & \vdots & & & \\ 1 & 0 & 0 & \cdots & 0 & 0 & 0 \end{array}\right]. \tag{32}$$

For the case of equally spaced measurement update intervals, the stacked $C$ matrices are

$$\begin{bmatrix} C[1] \\ C[2] \\ \vdots \\ C[n] \\ \hline C[n+1] \\ C[n+2] \\ \vdots \\ C[2n] \end{bmatrix} = \left[\begin{array}{ccccccc} 1 & 1 & 1 & \cdots & 1 & 1 & 1 \\ 0 & 0 & 0 & \cdots & 0 & 0 & 0 \\ & & & \vdots & & & \\ 0 & 0 & 0 & \cdots & 0 & 0 & 0 \\ \hline 1 & 1 & 1 & \cdots & 1 & 1 & 1 \\ 0 & 0 & 0 & \cdots & 0 & 0 & 0 \\ & & & \vdots & & & \\ 0 & 0 & 0 & \cdots & 0 & 0 & 0 \end{array}\right]. \tag{33}$$

Notice that the 0–1 structure in the $C$ matrices in Eqs. 32 and 33 reveals the measurement pattern. The ''1'' indicates a measurement update. The cross direction is indicated by different columns (in Eqs. 32 and 33), and the machine direction is represented by rows. Figure 6A shows the estimation errors for all 10 lanes in the cross direction. For example, at the first lane, the covariance starts increasing at $t > 61$ and the error drops as the first measurement comes in (at $t = 79$), and then the error goes up again until the next measurement becomes available at $t = 81$. The case of unequal sampling intervals ($T_1 = 18$ and $T_2 = 2$) leads to very different values in $\Sigma_{e,1}^{-}$ and $\Sigma_{e,2}^{-}$. At the center (5th or 6th lane), the sampling intervals are close to each other (Figure 2), and subsequently the worst estimation errors, $\Sigma_{e,i}$, are not too different from each other, as shown in Figure 6A (the dotted lines). On the other hand, the ideal sensor (Figure 5) gives exactly the same estimation errors for all 10 lanes (Figure 6B). Moreover, the stationary sensors show smaller error variances in estimation in terms of 2-norm or the $\infty$-norm. Figure 7A gives the worst estimation error for these two systems. The results show that the worst estimation error can be reduced significantly if the sampling intervals are equally spaced.

### *Control*

We have discussed the effect of measurement pattern on estimation thus far. A more realistic measure should be such

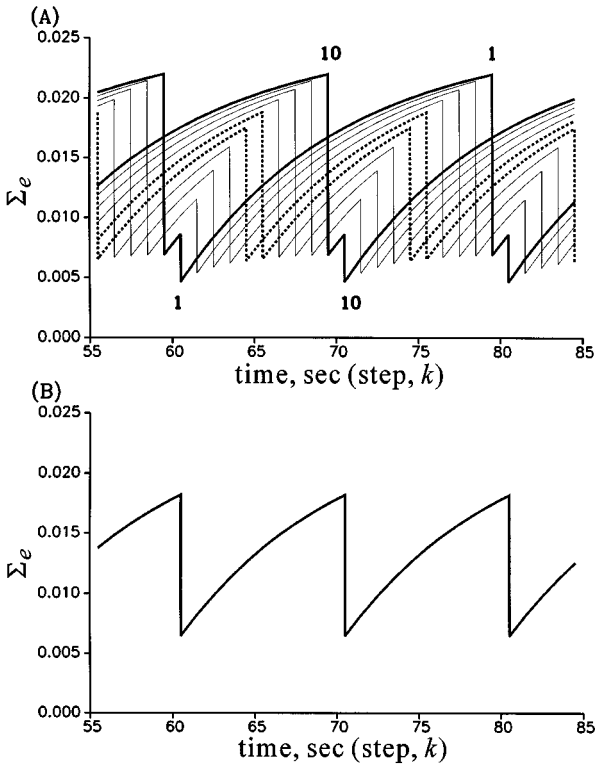


**Figure 6. Variances of estimation.**

(A) Scanning sensor with linear sweep and (B) stationary sensors for all 10 lanes on the cross direction.

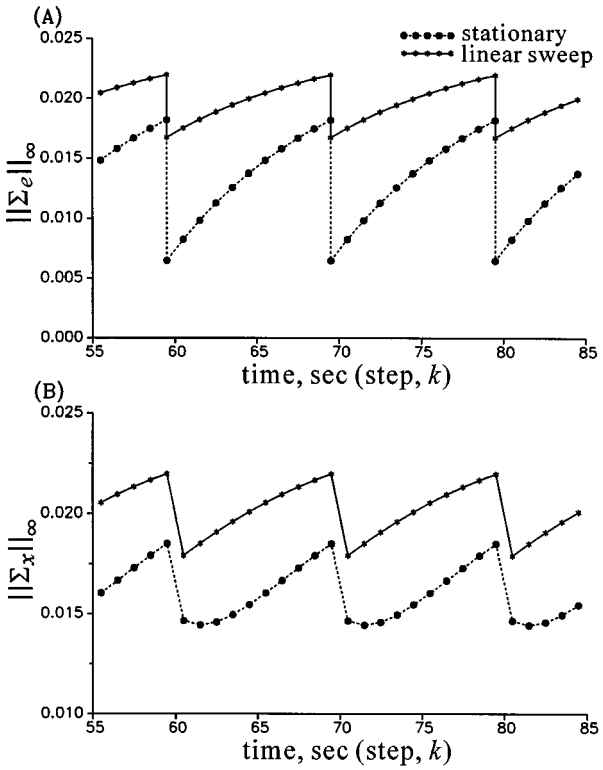


**Figure 7. ∞-Norm of variances with linear scanning sensor and stationary sensors.**

(A) Estimation and (B) LQG control.

an effect on control performance. That is, the effect of measurement pattern on the variation of film properties. Consider the discrete time system in Eqs. 3 and 4 with the Kalman filter Eqs. 5–9. An LQG control is employed (Åström and Wittenmark, 1990). The LQG control minimized the following objective function:

$$\min_u J = x^T \mathbf{\Omega} x + u^T \Gamma u, \tag{34}$$

where $\mathbf{\Omega}$ and $\mathbf{\Gamma}$ are the weightings for the states ($x$) and input ($u$), respectively. The controller then becomes

$$u[k] = -F[k]\hat{x}[k|k-1], \tag{35}$$

with the controller matrix $F$

$$F[k] = \left(\Gamma + B[k]^T S[k] B[k]\right)^{-1} B[k]^T S[k] A[k], \tag{36}$$

where $S$ can be obtained from the Riccati equation:

$$S[k+1] = A[k]^T S[k] A[k] - A[k]^T S[k] B[k]\left(\Gamma + B[k]^T S[k] B[k]\right)^{-1} B[k]^T S[k] A[k] + \mathbf{\Omega}. \tag{37}$$

The state estimation under feedback then can be expressed as

$$\hat{x}[k+1|k] = (A[k] - B[k]F[k])\hat{x}[k|k-1] + A[k]K[k](C[k]e[k|k-1] + v[k]). \tag{38}$$

From the definition of the estimation error, we have:

$$\mathbf{\Sigma}_x[k] = \mathbf{\Sigma}_e[k|k-1] + \mathbf{\Sigma}_{\hat{x}}[k|k-1], \tag{39}$$

where $\mathbf{\Sigma}_{\hat{x}}[k|k-1]$ is of the form

$$\Sigma_{\hat{x}}[k|k-1] = (A[k-1] - B[k-1]F[k-1])\Sigma_{\hat{x}}[k-1|k-2](A[k-1] - B[k-1]F[k-1])^T + A[k-1]K[k-1](C[k-1]\mathbf{\Sigma}_e [k-1|k-2]C[k-1]^T + R[k-1])K[k-1]^T A[k-1]^T. \tag{40}$$

Equations 39 and 40 clearly indicate that the covariances of estimation error ($\mathbf{\Sigma}_e$) affects that of control error ($\mathbf{\Sigma}_x$).

Let us use the example in the previous section to illustrate this. Assume that the weightings in the LQG are $\mathbf{\Omega} = I$ and $\mathbf{\Gamma} = 0.1I$, respectively. The variances of the control error ($\mathbf{\Sigma}_x$) can be calculated. The results show that, for the scanning sensor with a zig-zag pattern, the behavior of the variances of control error are fairly similar to that of the estimation error. The variance of control increases with time until the next

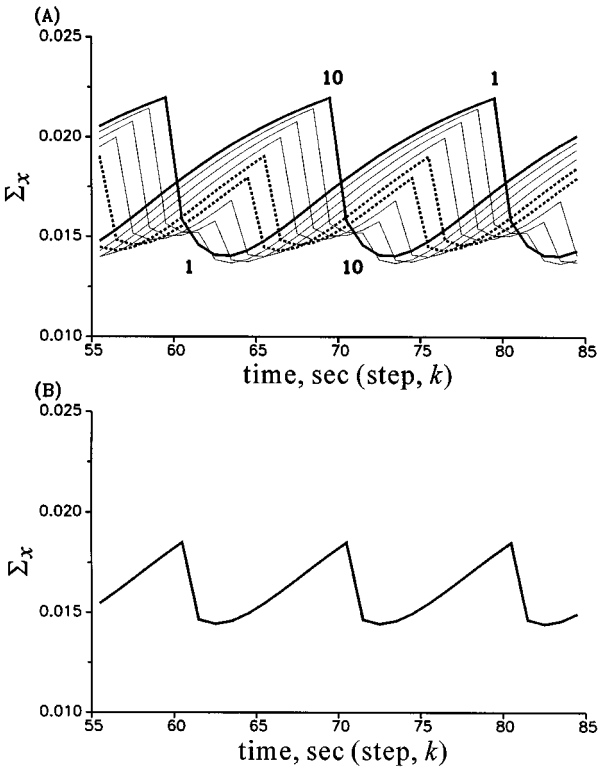


**Figure 8. Variances of LQG control for all 10 lanes in the cross direction.**

(A) Linear scanning sensor and (B) stationary sensors.

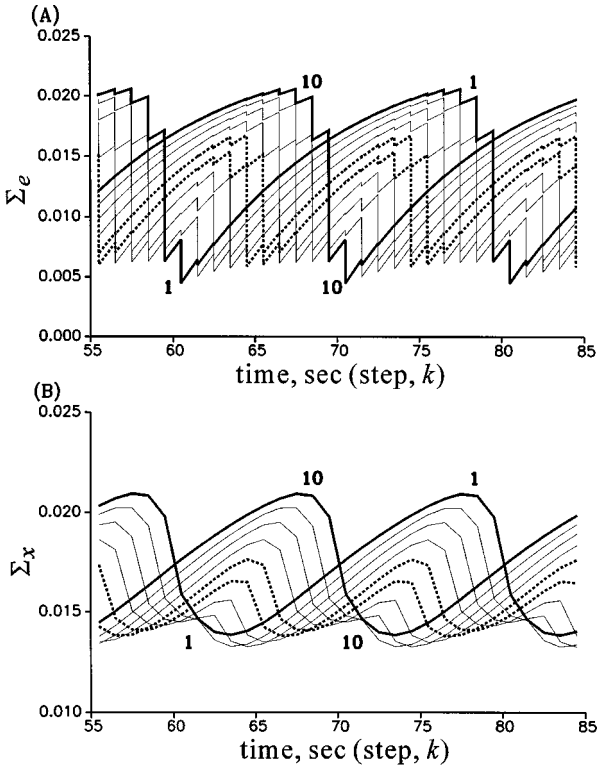


**Figure 10. Variances for system with with $\rho_s = 0.6$.**

(A) Estimation and (B) LQG control.

measurement becomes available (Figure 8A). On the other hand, the stationary sensors give identical performance across the CD. This is illustrated nicely in Figure 9, where the averaged variances of the control error ($\bar{\Sigma}_x$) are plotted in the cross direction. As expected, improvement can be made across the CD except around the center (since the measurement update intervals are approximately the same). Control performance becomes poorer toward the edges when the scanning sensor is used. The stationary sensors show uniformity along the cross direction. Moreover, the worst variances in control (Figure 7B) are even larger for the conventional scanning sensor. This has an important implication from the product quality-control point of view, since we could have weak spots on the sheet (such as polymer film) that are generally unacceptable for the 2-D products.

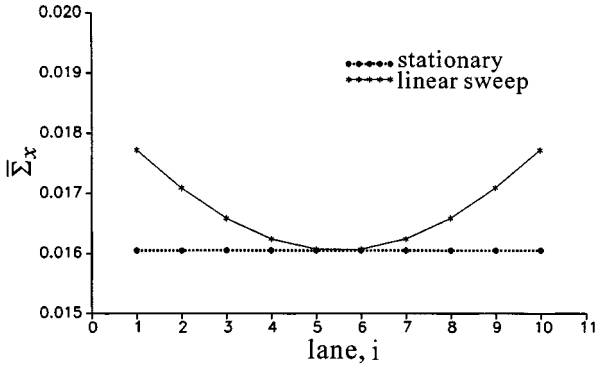


**Figure 9. Averaged variances of LQG control for two different sensor arrangements: linear sweep and stationary sensors.**

Up to this point, we assume process noises only affect a specific lane, that is, $\rho_s = 0$. In practice, noises will propagate in the cross direction and eventually level off, that is, $0 < \rho_s < 1$. Let us take $\rho_s = 0.6$ for the same example to compare different sensor arrangements. Figure 10 shows that both the estimation and control errors are smaller as compared to the case of $\rho_s = 0$. However, characteristics from unequally spaced sampling intervals remains. That is, poor estimation and control are expected toward the edges.

## Improved Sensor Trajectory

As mentioned in the previous section, performance degradation in the estimation and, consequently, control is due to the unequal measurement update intervals and poor performance is observed at edges where the two intervals ($T_1$ and $T_2$) differ significantly. This is the consequence of the sensor arrangement since the scanning sensor moves back and forth in the cross direction with a constant speed. Two approaches can be taken to improve the performance. One is to increase the number of sensors, and a larger number of stationary sensors can eliminate all the problems associated with the unequal measurement update intervals. The other approach is to adjust the trajectory of the sensor such that the difference of the measurement update intervals is reduced when a single sensor is employed. The second approach is taken here.

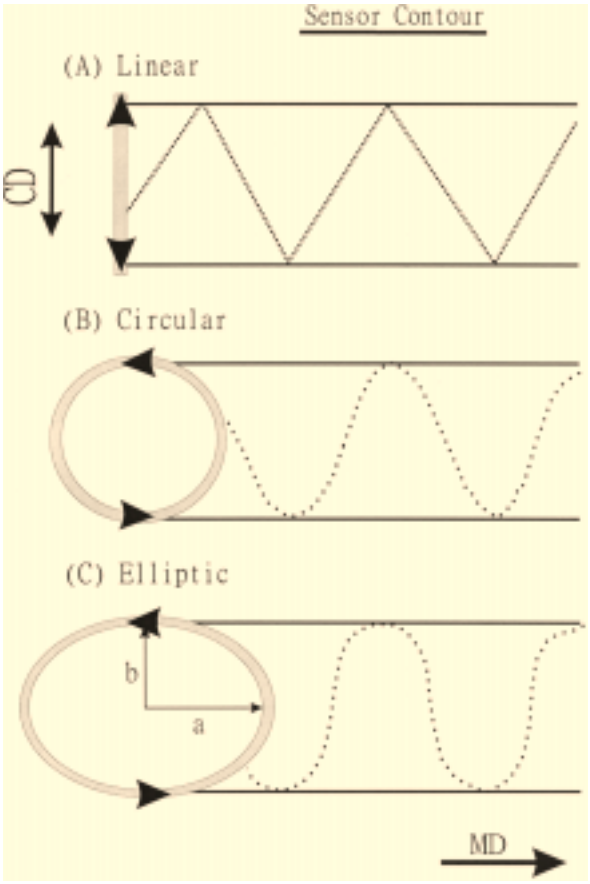


**Figure 11. Scanning sensor with (A) linear, (B) circular, and (C) elliptic contours.**

*Concept of elliptic contour*

The ultimate goal is to make the measurement update intervals equal to each other (that is, $T_1 = T_2$). Unfortunately, this cannot be done using a single scanning sensor moving along a closed contour. At best, we can redesign the contour such that $T_1$ and $T_2$ are less unequal. A simple way to achieve that is to let the sensor move along an elliptic (or circular) contour such that more time is spent on the edges (Figure 11). This led to a sine-wave-like trajectory instead of a zig-zag trajectory. Notice that, unless otherwise mentioned, we assume the sensor moves with a constant speed.

Since the trajectory on the MD is a periodical function, we can just look at a specific period. The sensor trajectory is defined on the Cartesian coordinate, where the $x$-axis defines the time and the $y$-axis defines the cross direction. Assume that the origin, $(0,0)$, is placed on the edge of the sheet and that the width is $2b$. Consider a scanning sensor with the linear sweep (Figure 11A). For a given period, the zig-zag trajectory can be described by a piecewise-linear function:

$$y_{CD} = \begin{cases} 4b \cdot \dfrac{t}{T}, & 0 \le t < \dfrac{T}{2} \\ 2b - 4b \dfrac{\left(t - \dfrac{T}{2}\right)}{T}, & \dfrac{T}{2} \le t \le T, \end{cases} \tag{41}$$

where $T$ is the full period and $y_{\mathrm{CD}}$ stands for position in the CD starting from the bottom edge. The position in the machine direction is simply a linear function in time:

$$x_{MD} = v_p \cdot t, \tag{42}$$

where $x_{MD}$ is the position in the MD and $v_p$ is the speed of the sheet. Therefore, the profile can be obtained by substituting Eq. 42 into Eq. 41:

$$y_{CD} = \begin{cases} 4b \cdot \dfrac{x_{MD}}{v_p T}, & 0 \le x_{MD} < \dfrac{v_p T}{2} \\ 2b - 4b \dfrac{x_{MD}}{v_p T}, & \dfrac{v_p T}{2} \le x_{MD} \le v_p T. \end{cases} \tag{43}$$

If the sensor moves on a circular contour, as shown in Figure 11B, then, instead of a zig-zag pattern, the trajectory becomes a sine wave. Consider a sheet with a width of $2b$ and where the origin is located on the midpoint. The relationship between $y_{\mathrm{MD}}$ and time is simply

$$y_{CD} = b \cdot \sin\left(2\pi \frac{t}{T}\right). \tag{44}$$

And, for a constant speed in the MD (that is, $v_p$), the trajectory becomes

$$y_{CD} = b \cdot \sin\left(2\pi \frac{x_{MD}}{v_p T}\right). \tag{45}$$

This is exactly what we have in Figure 11B. Comparing Eq. 45 to Eq. 43, or Figure 11B and Figure 11A, it becomes evident that the difference between the two measurement update intervals is reduced, especially toward both edges. The difference can further be reduced, if the sensor moves on an elliptic contour with a major axis $2a$ on the MD, and a minor axis $2b$ on the CD (Figure 11C). Figure 12 compares the scanning trajectories for the linear, circular, and elliptic ($a/b = 2$) contour. Since we assume a constant speed for the sensor ($v_s$), it is not possible to obtain a closed-form solution for the elliptic contour. However, the case of constant angular velocity gives a good approximation, provided the eccentricity

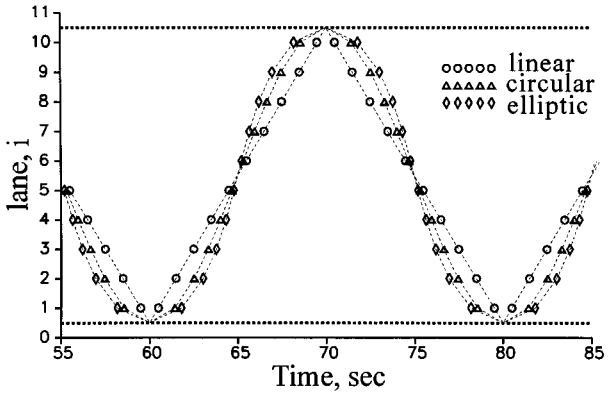


**Figure 12. Sensor trajectories for linear, circular and elliptic contours.**

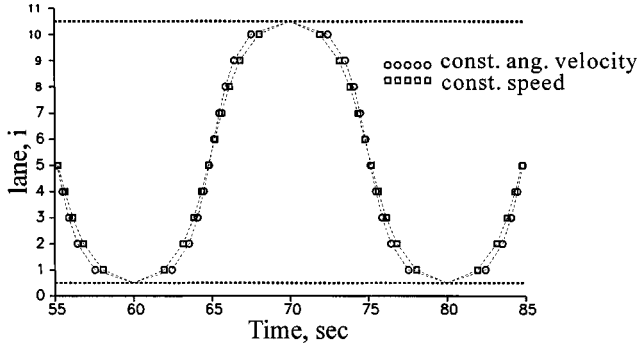


**Figure 13. Sensor trajectories for elliptic contour: constant speed vs. constant angular velocity.**

($\epsilon = \sqrt{a^2 - b^2}/a$) is not too large. The distance between the center and a given point on the periphery is

$$r = \frac{ab}{\sqrt{a^2 \sin^2\theta + b^2 \cos^2\theta}}, \tag{46}$$

where $\theta$ denotes the angle away from the major axis (Figure 11C). The position on the CD, $y_{CD}$, can be described by $y_{CD} = r \cdot \sin\theta$. Substituting $2\pi t/T$ for $\theta$, the position on the cross direction then becomes

$$y_{CD} = \frac{ab}{\sqrt{a^2 \sin^2\left(\frac{2\pi t}{T}\right) + b^2 \cos^2\left(\frac{2\pi t}{T}\right)}} \cdot \sin\left(\frac{2\pi t}{T}\right). \tag{47}$$

The trajectory can be obtained by simply substituting $x_{MD}/v_p$ for $t$:

$$y_{CD} = \frac{ab}{\sqrt{a^2 \sin^2\left(\frac{2\pi x_{MD}}{v_p T}\right) + b^2 \cos^2\left(\frac{2\pi x_{MD}}{v_p T}\right)}} \times \sin\left(\frac{2\pi x_{MD}}{v_p T}\right). \tag{48}$$

For the case of $a/b = 2$, Figure 13 shows that Eq. 48 gives a good approximation for the trajectory. The analytical results presented here are useful in the design of sensor contours.

For the case of elliptic sensor contour, several characteristics can be observed. Despite the assumption of constant sensor speed for the linear sweep, the sensor actually starts from a stationary position and moves forward, presumably with a constant speed, followed by braking such that it stopped at the other end and the process is repeated for the backward sweep. Therefore, motor on top of carriage performs the acceleration and braking repeatedly. On the other hand, for the case of elliptic (or circular) contour, the sensor simply travels along the ellipse (or circle) with a constant speed (without any acceleration or braking). The other difference between the two is we assume that it takes the same amount of time to complete two measurement updates for a given CD position. This implies that the sensor should move faster (that is, larger $v_s$) for the elliptic (or circular) contour. However, the sensor collects the same amount of data points in the same full period ($T$). In other words, for the case of the elliptic contour, the speed of the sensor has to be higher to complete a full cycle of scanning and the data points are unequally distributed along the cross direction. This should cause little problem, since the number of data points collected in a half-period is far greater than the number of actuators. Table 1 shows the speed ratios for different $a/b$ ratios. For the case of circular contour, the sensor travels at a speed 1.57 times that of the linear sweep (that is, $v_s/v_s^o = 1.57$).

**Table 1. Velocity Ratios for Different Contours**

| | Linear* | Circular | Elliptic** |
|---|---|---|---|
| $\frac{v_s}{v_s^o}$ | 1 | 1.57 | 2.42 |

*Normalized with respect to the speed of linear sweep.
**$a/b = 2$.

Next, the control performance of different sensor arrangements is compared. Again, consider the example in the section on estimation and control, with $\rho_s = 0.6$. The averaged variances of the control error ($\overline{\Sigma}_x$) in the CD and MD directions are employed. Figure 14 shows that the elliptic sensor contour gives better control over the linear sweep. The performance of the circular contour is about the same as that of the elliptic contour in the cross direction, as shown in Figure 14A. For the variances in the machine direction (taking the

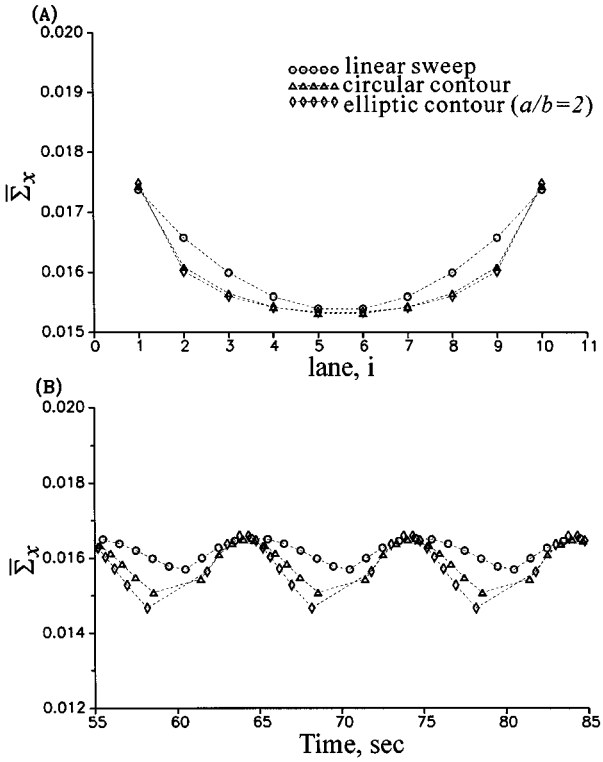


**Figure 14. Averaged variances of LQG control for different sensor arrangements.**
(A) Cross direction and (B) machine direction.

average for all lanes), the scanning sensor with the elliptic contour again shows better control over the conventional arrangement (Figure 14B). Notice that, in terms of the CD direction, the improvement is evident across the cross direction except for the center and both edges (Figure 14A). The results presented here show that better control can be obtained with a scanning sensor with an elliptic contour. Moreover, the sensor with an elliptic contour has the advantage of traveling at a constant speed, which requires less service attention. However, this new arrangement needs a complete revamping of the carriage for existing processes.

### *Linear sweep with acceleration*

The elliptic contour is not the only way to obtain the trajectory in Figure 11B and 11C. A simple alternative is to acceleration (or decelerate) the scanning sensor while traveling back and forth on a linear carriage. This can be achieved by reprogramming the variable-speed motor.

Assume that it takes the same full period $T$ to complete a forward and backward sweep and that the sensor is accelerated or decelerated with an acceleration $a$. The sensor starts at the bottom edge (such as Figure 11A) and it accelerates with $a$ to the midpoint. Then the sensor decelerates with $a$ until it reaches the edge on the top and the speed becomes zero at this point. The sensor repeats the acceleration–deceleration cycle on the linear carriage in each $T/2$ period. Since it takes $T/4$ to reach the midpoint of a width of $2b$, the acceleration then becomes

$$\mathrm{a} = \frac{32b}{T^2}. \tag{49}$$

The trajectory then becomes

$$y_{CD} = \begin{cases} \dfrac{16b}{T^2}t^2, & 0 \le t < \dfrac{T}{4} \\ -2b + \dfrac{16b}{T}t - \dfrac{16b}{T^2}t^2, & \dfrac{T}{4} \le t \le \dfrac{T}{2}. \end{cases} \tag{50}$$

Figure 15 shows that scanning sensor with an acceleration–deceleration cycle is almost the same as the result of a circular contour. It should be emphasized that the trajectory is obtained using a conventional linear sweep with acceleration (such as Eq. 50). Obviously, improved control performance can be achieved with this variable-speed scanning sensor. Figure 16 shows that improvement in the averaged variances in both the CD and MD directions as compared to the constant-speed scanning sensor. The variable-speed scanning sensor provides an attractive alternative to achieve better control. More importantly, it can be implemented by reprogramming the motor on the carriage.

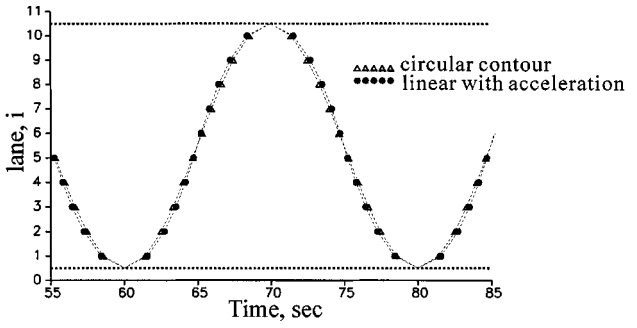


**Figure 15. Trajectories for sensors with circular contour with constant speed vs. linear sweep with acceleration–deceleration.**

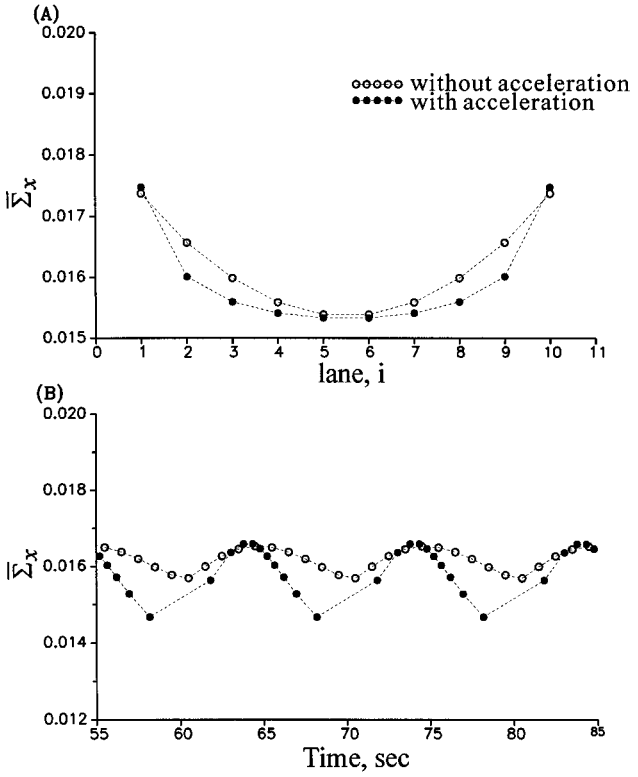


**Figure 16. Averaged variances of LQG control for different sensor arrangements.**

(A) Cross direction and (B) machine direction.

### *Alternative sensor arrangements*

In addition to modifying sensor trajectory, several alternatives exist for improved estimation and control. One obvious choice is to increase the sampling rate of the scanning sensor (such as equipped with an improved radiation-emitting source and corresponding detector) while maintaining the traveling speed. That means we have more data points in a full period $T$ (Figure 17). If we choose to fasten the rate for estimation and control, the results, doubled sampling rate, in Table 2, indicate that only a little improvement in estimation (and control) errors can be achieved. Actually, this is within one's expectation, since maintaining a constant traveling speed for the scanning sensor does not resolve the imbalance in the measurement update intervals (such as $T_1$ and $T_2$), and therefore the improvement is only marginal. A second alternative is to increase both the sampling rate and the traveling speed of the sensor (with appropriate technology), as shown in Figure 17. Table 2 shows that much smaller variances are

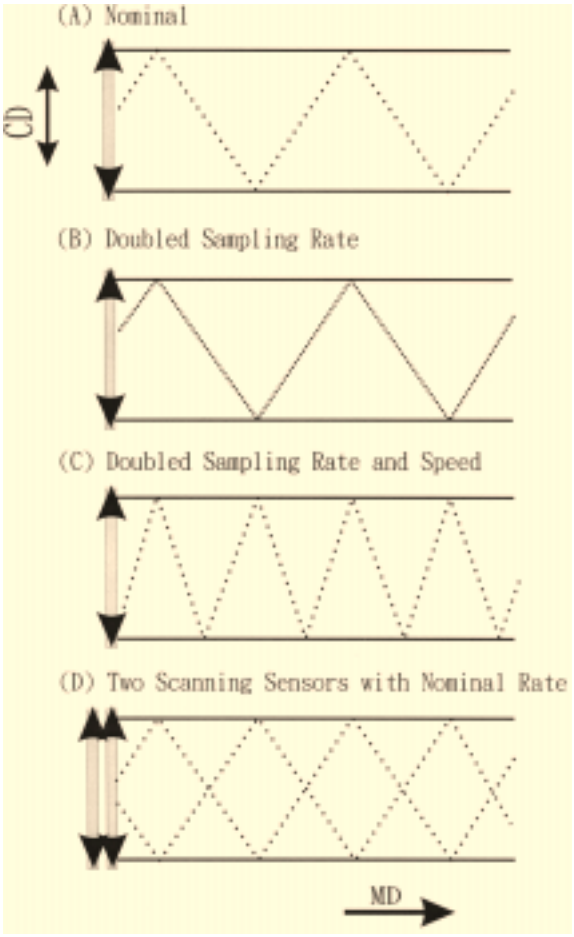


**Figure 17. Alternative sensor arrangements.**

(A) Nominal sampling rate and traveling speed; (B) doubled sampling rate with nominal traveling speed; (C) doubled sampling rate and traveling speed; and (D) two sensors traveling in the opposite direction with nominal sampling rate and traveling speed.

obtained, since the period $T$ is halved (with a doubled speed) and, subsequently, the difference between $T_1$ and $T_2$) is shortened. The comparison made here is consistent with our earlier observation: performance degradation in the estimation and control is due to the unequal measurement update intervals. More importantly, it offers a clear direction for future sensor development.

At the present stage, however, if improvement ought to be sought for better control with currently available sensors, what are the options? A straightforward approach is to put in an additional sensor (or sensors). The next question naturally arises: What is the arrangement for these two sensors? Should they travel in the same diretion or the opposite direction, sweep the entire CD range, or half of the distance? Figure 17 shows one of the better solutions to the problem: the sensors should travel in the opposite direction while sweeping the entire cross direction (Chang, 1998). The results show that the estimation and control errors are comparable to that of much advanced sensor.

In terms of sensor arrangement, the results presented here offer several attractive alternatives for better estimation and control in sheet-forming process. The decision on any possible revamping clearly depends on the current sensor settings in the plant and the expectation of future sensor development. It should be emphasized again, however, that any attempt to eliminate the imbalance in the measurement update intervals will improve control performance.

## Conclusions

In this article, we present an approach to improved control for the sheet-forming process. Instead of reconstructing the state for a given measurement pattern, we redesign the sensor trajectory such that better properties in estimation can be obtained. First, the characteristics of the conventional scanning sensor are explored and implications to the estimation and control are also investigated. Then, the concept of elliptic sensor contour is proposed, and analytical expression for the sensor trajectories are also derived. In addition, the concept of the elliptic sensor contour can be implemented as a variable-speed sensor, which requires only minor modification of the existing sensor. Control performance of the proposed sensor arrangements is demonstrated favorably via simulation. Moreover, several alternative sensor arrangements are evaluated. They offer clear guidelines to achieve better estimation and control.

## Acknowledgments

This work was supported by the National Science Council of Taiwan under Grant NSC86-2214-E011-009. We thank, the anonymous reviewers for their suggestions, which led to the development of the subsection titled ''Alternative Sensor Arrangements.''

## Literature Cited

Åström, K. J., and B. Wittenmark, *Computer-Controlled Systems: Theory and Design*, 2nd ed., Prentice Hall, Englewood Cliffs, NJ (1990).

Bergh, L. G., and J. F. MacGregor, ''Spatial Control of Sheet and Film Forming Processes,'' *Can. J. Chem. Eng.*, **65**, 148 (1987).

Braatz, R. D., M. L. Tyler, M. Morari, F. R. Pranckh, and L. Sartor, ''Identification and Cross-Directional Control of Coating Processes,'' *AIChE J.*, **38**, 1329 (1992).

Bryson, A. E., and Y. C. Ho, *Applied Optimal Control*, Hemisphere, New York (1975).

Chang, D. M., ''Coordinated Control for Two-Dimensional Space,'' PhD Diss., National Taiwan Univ. of Science and Technology, Taipei (1998).

Chen, S.-C. ''Full-Width Sheet Property Estimation from Scanning Measurements,'' *Proc. Control System'92*, Whistler, BC (1992).

**Table 2. 2-Norm and ∞-Norm of Errors for Different Sensor Arrangements with Linear Sweep**

| | $\Sigma_e$ | | $\Sigma_x$ | |
|---|---|---|---|---|
| | 2-Norm | ∞-Norm | 2-Norm | ∞-Norm |
| Nominal | 0.0131 | 0.0206 | 0.0162 | 0.0210 |
| Doubled sampling rate | 0.0124 | 0.0202 | 0.0155 | 0.0206 |
| Doubled sampling rate and sweeping speed | 0.0096 | 0.0156 | 0.0134 | 0.0165 |
| Two sensors with nominal rate and speed | 0.0094 | 0.0147 | 0.0137 | 0.0160 |

Chen, S.-C., and R. J. Pfeifer, "Papermaking Results Using HyperScan: A Full Sheet Imaging System," *Proc. Process and Product Quality Conf.*, Milwaukee, WI, p. 151 (1998).
Chen, S.-C., and R. G., Wilhelm, Jr., "Optimal Control of Cross-Machine Direction Web Profile with Constraints on the Control Effort," *Proc. Amer. Control. Conf.*, Seattle, WA (1986).
Dave, P., F. J. Doyle III, and J. F. Pekny, "Customization Strategies for the Soution of Linear Programming Problems Arising from Large Scale Model Predictive Control of a Paper Machine," *J. Process Control*, **9**, 385 (1999).
Dave, P., D. A. Willig, G. K. Kudva, J. F. Pekny, and F. J. Doyle, "LP Methods in MPC of Large-Scale Systems: Application to Paper-Machine CD Control," *AIChE J.*, **43**, 1016 (1997).
Grewal, M. S., and A. P. Andrews, *Kalman Filtering: Theory and Practice*, Prentice Hall, Englewood Cliffs, NJ (1993).
Laughlin, D. L., M. Morari, and R. D. Braatz, "Robust Performance of Cross-Directional Basis-Weight Control in Paper Machines," *Automatica*, **29**, 1395 (1993).
Mayback, P. S., *Stochastic Models, Estimation and Control*, Academic Press, New York (1979).
Rawlings, J. B., and I.−L. Chien, "Gage Control of Film and Sheet Forming Processes," *AIChE J.*, **42**, 753 (1996).
Rigopoulos, A., Y. Arkun, and F. Kayihan, "Identification of Full Profile Disturbance Models for Sheet Forming Process," *AIChE J.*, **43**, 727 (1997).
Shapiro, S. L., "Metered Size Press Optimization via Measurement and Control," *Proc. TAPPI Metered Size Press Forum*, New Orleans, LA, p. 173 (1998).
Tyler, M. L., and M. Morari, "Estimation of Cross-Directional Properties: Scanning vs. Stationary Sensors," *AIChE J.*, **41**, 846 (1995).
Van Antwerp, J. G., and R. D. Braatz, "Model Predictive Control of Large Scale Processes," *J. Process Control*, **10**, 1 (2000).
Wang, X. G., G. A. Dumont, and M. S. Davies, "Estimate in Paper Machine Control," *IEEE Control Syst. Mag.*, **13**, 34 (1993).

## Appendix A

Substituting Eq. 25 into Eq. 27, the objective function becomes:

$$J=\int_0^{T-T_1}\left[e^{2A_ct}\Sigma_e^+(T_1)+\frac{Q_c}{2A_c}(e^{2A_ct}-1)\right]dt + \int_0^{T_1}\left[e^{2A_ct}\Sigma_e^+(T-T_1)+\frac{Q_c}{2A_c}(e^{2A_ct}-1)\right]dt. \quad \text{(A1)}$$

After some algebraic manipulation, we have

$$J=\frac{1}{2A_c}\left[e^{2A_cT_1}\Sigma_e^+(T-T_1)+e^{2A_c(T-T_1)\Sigma_e^+(T_1)}\right] - \frac{1}{2A_c}\left[\Sigma_e^+(T_1)+\Sigma_e^+(T-T_1)\right] + \frac{Q_c}{4A_c^2}\left[e^{2A_cT_1}+e^{2A_c(T-T_1)}\right]-\frac{Q_c}{2A_c^2}-\frac{Q_cT}{2A_c}. \quad \text{(A2)}$$

Taking the derivative of Eq. A2, we obtain

$$\frac{\partial J}{\partial T_1}=\frac{1}{2A_c}\left[e^{2A_cT_1}\frac{\partial\Sigma_e^+(T-T_1)}{\partial T_1}+e^{2A_c(T-T_1)}\frac{\partial\Sigma_e^+(T_1)}{\partial T_1}\right] + \left[e^{2A_cT_1}\Sigma_e^+(T-T_1)-e^{2A_c(T-T_1)}\Sigma_e^+(T_1)\right] - \frac{1}{2A_c^2}\left[\frac{\Sigma_e^+(T_1)}{\partial T_1}+\frac{\Sigma_e^+(T-T_1)}{\partial T_1}\right] + \frac{Q_c}{2A_c^2}\left[e^{2A_cT_1}-e^{2A_c(T-T_1)}\right]. \quad \text{(A3)}$$

In Eq. A3, the items of the bracket become zero when $T_1 = T/2$. That implies a minimum.

*Manuscript received Apr. 26, 1999, and revision received Mar. 3, 2000.*